1

Do heterogenous firing responses lead to diverse couplings to presynaptic activity ?

Y. Zerlaut[1] & A. Destexhe[1]

March 15, 2016

I   Abstract

Neocortical processing of sensory input rely on the specific activation of subpopulations within the cortical network. Though specific circuitry is thought to be the primary mechanism underlying this functional principle, we investigate here a putative complementary mechanism: whether diverse biophysical features in single neuron contribute to such differential activation.

In a companion study (Zerlaut et al., 2016), we reported that, in young mice visual cortex, individual neurons differ not only in their excitability but also in their sensitivities to the properties of the membrane potential fluctuations. In the present work, we analyze how this heterogeneity is translated into diverse input-ouput properties (i.e. in the relation from presynaptic quantities to spiking probability) in the context of low synchrony population dynamics.

To this purpose, we designed a simplified morphological model of layer V pyramidal neurons with a dendritic tree following Rall's branching rule. We first show that we are able to calibrate this simplified model on *in vitro* measurements of somatic input impedance. We then propose an analytical derivation for the membrane potential fluctuations at the soma as a function of the properties of the synaptic bombardment. This mathematical description allows to easily emulate various forms of presynaptic activities: either balanced, unbalanced, synchronized, purely proximal or purely distal synaptic activity.

We found that those different forms of activity led to various comodulations of the membrane potential fluctuation properties, thus raising the question whether individual neurons might differentially couple to specific forms of activity because of their various firing responses to fluctuations.

We indeed found such an heterogenous response, but trivially, the only significant contribution to the various firing response was the different levels of cellular excitability. A notable exception appeared for proximal activity: increasing proximal activity could either promote firing response in some cells or suppress it in some other cells whatever their individual excitability. This behavior could only be explained by various sensitivities to the speed of the fluctuations, that was previously linked to heterogenous levels of sodium inactivation and sodium channels density.

In addition to giving quantitative insight on the impact of various excitability levels in individual neurons, the present study suggests a new functional impact of biophysical heterogeneity: various levels of density of sodium channels and sodium inactivation will control the response of individual neurons to proximal activity.

II   Introduction

Neocortical processing of sensory input rely on the specific activation of subpopulations within the cortical network. The details of how such specific activations happens are key questions in systems neuroscience.

The neocortex is characterized by some degree of specific circuitry: neurons differ in their afferent connectivity: e.g. in the somato-sensory cortex of rodents, simple cells layer IV neurons in the visual cortex, barrels sample inputs from different locations in the thalamus nucleus *ref?*. Neocortical neurons also vary in their electrophysiological properties: for example, heterogenous levels in the action potential threshold are routinely measured both in vivo *Nowak, etc* and in vitro *refs*. An emerging picture is that the sensitivity of a neuron to a given feature results from the combination of its *circuit specificity* (relative to this feature) and its *biophysical specificity*. The somato-sensory cortex study of Crochet et al. (2011) illustrates this point precisely. During active touch, the response probability of a neuron (its sensitivity to whisker touch) follows from the combination of the reached level of synaptically-driven membrane potential deflection (resulting from its *circuit-specificity*) and its threshold for action potential triggering (its *biophysical specificity*). The same result hold for texture recognition in the study of Yang et al. (2015) where the combination of the two mentionned effect correlated with the *xx, to be checked* in barrel cortex neurons. Those results therefore suggest that heterogeneity in the electrophysiological or biophysical properties of neocortical neurons might have an impact on their functional role during sensory processing *note nonetheless a factor 2-3 between the ranges of each effect*.

In the present work, we further investigate this putative interaction in the light of the variability in the biophysical features reported in our companion communication, namely that single neurons in juvenile mice cortex not only vary in their excitability (linked to the action potential threshold, see *xx*) but also in their sensitivity to the properties of the membrane potential fluctuations. Our previous communication introduced those new dimensions in the *biophysical specificity* and we now aim at understanding their functional impact.

To highlight the impact of the *biophysical specificity*, we will investigate single neuron response in a framework where the *circuit specificity* is null, i.e. with the hypothesis

that all neurons sample statistically equally.

In the context of low synchrony population dynamics characterizing the activity of activated cortical states, information processing through population rate correspond to the temporal modulations of the membrane potential fluctuations.

Here specific form of presynaptic stimulation that are well defined in a framework

Within the context of population dynamics, where the neuronal response can be described as a spiking probability and the input can be described by stationary firing rates (or slowly modulated firing rates compared to the membrane time constant).

We designed a theoretical model for passive dendritic integration that allows an analytical treatment and thus easily enables the implementation of various types of presynaptic activity. It is based on a symmetrical morphology where branching follows the Rall's 3/2 exponent rule (Rall, 1962), the analytical derivation relies on adapting the equivalent cylinder transformation (Rall, 1962) to the properties of the high conductance state (Destexhe et al., 2003).

We implemented various types of presynaptic activity: either unbalanced, purely proximal, purely distal or synchronized. We found that those various types of activity corrresponds to different variations of the properties of the membrane potential fluctuations (mean depolarization, standard deviation and autocorrelation time). The various firing responses (as a function of the fluctuation properties) for individual neurons found in our companion study then led to diverse coupling to each activity type.

We suggested in our companion study that the properties of the fluctuations could follow various comodulations depending on the type of presynaptic activity, what we demonstrate in this study.

III Results

The results are organized as follows. We first formulate our theoretical framework for cellular computation which arbitrarily separate the question of dendritic integration and spiking probability. Then we present our simplified model of dendritic morphology which we calibrated on *in vitro* measurements. We derive an analytical approximation for the membrane potential fluctuations at the soma that we compare to numerical simulations using standard compartemental modeling. We implement various types of presynaptic activity and *xx*

III.1 A theoretical framework for single cell computation in the fluctuation-driven regime

In the fluctuation-driven regime, the cellular input-output function of a neocortical neuron corresponds to the function that maps the presynaptic variables to the spiking probability of the neuron (this is true both in a rate coding paradigm (**?**; **?**) or in a stochastic temporal coding paradigm (Rossant et al., 2011)). In addition, because our study focuses on effects resulting from population
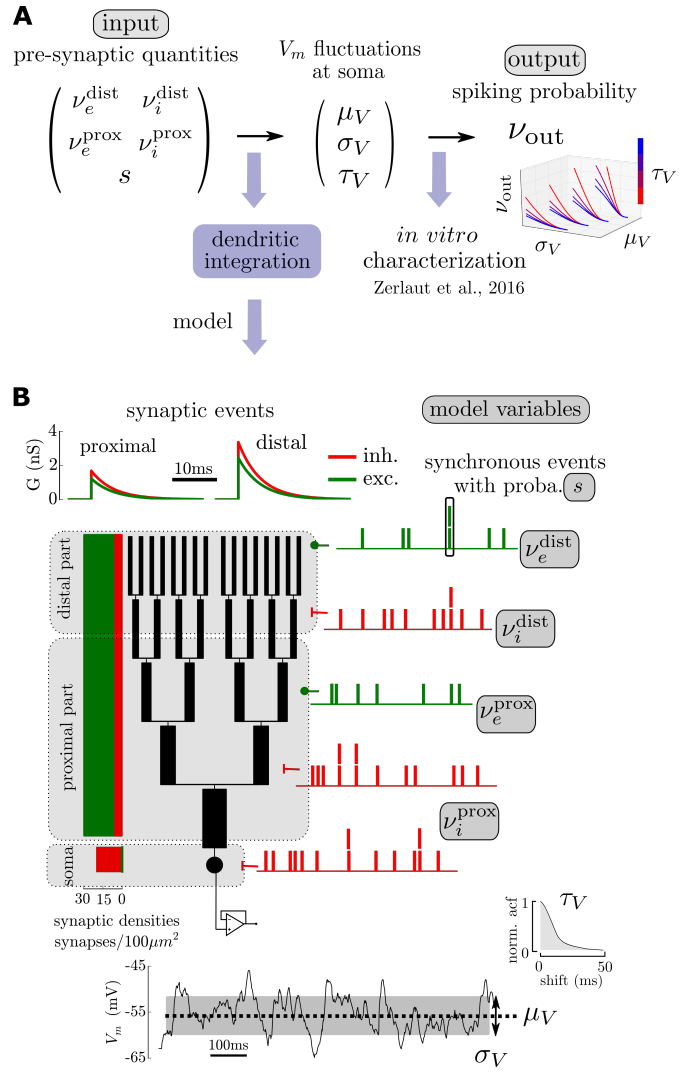
Figure 1: A theoretical framework for single cell computation in the fluctuation-driven regime. **(A)** Theoretical paradigm: to get the input-output function of a single cell, we split the relation from presynaptic quantities (the input) to the spiking probability (the output) into two steps. 1) passive dendritic integration shape the membrane potential at the soma and 2) how those fluctuations are translated into spikes is captured by a firing response function determined *in vitro* (Zerlaut et al., 2016) **(B)** Theoretical model for dendritic integration. A single cell is made of a lumped impedance somatic compartment and a dendritic tree. The dendritic tree is composed of B branches (here B=5), the branching is symmetric and follow Rall's 3/2 rule for the branch diameters. Synapses are then spread all over the membrane according to physiological synaptic densities. We define 3 domains: a somatic and proximal domain as well as a distal domain, excitatory and inhibitory synaptic input can vary independently in those domains. An additional variable: synaptic synchrony controls the degree of coincidents synaptic inputs.

dynamics, the presynaptic variables will have a simple description: firing rates and a synchrony degree.

III.2 A simplified morphological model for dendritic integration

The morphology of our theoretical model is a lumped impedance somatic compartment in parallel with a dendritic arborization of symmetric branching following Rall's 3/2 branching rule (see Figure 1B and Methods V.1). This morphology is of course a very reductive description of pyramidal cells: it does not discriminate between the distinct apical trunk and the very dense basal arborization. Also, branching in pyramidal cell morphologies have been shown to deviate from Rall's 3/2 branching rule. Nonetheless this simplified model contains the important ingredient for our study: the fact that the transfer impedance to the soma of a synaptic input will strongly depend on its location on the dendritic tree. Indeed, as observed experimentally (Magee, 2000), distal events will be more low-pass filtered than proximal events in this model.

from (Spruston, 2008): *Usually, proximal dendrites receive excitatory inputs from local sources (collaterals in the same area or from an adjacent area) whereas the distal apical tuft receives inputs from more distant cortical and thalamic locations (FIG. 1b).*

We spread synapses onto this morphology according to physiological densities (taking lower bounds of **?**) and describe synaptic events as transient permeability changes of ion-selective channels (see Methods V.2). We arbitrarily separate the dendritic tree into two domains: a proximal and a distal domain. Following experimental evidences (Magee, 2000), we set a higher synaptic efficacy for distal synapses. The synaptic parameters take physiological values (Destexhe et al., 1998) and can be found on Table 1. The passive and morphological parameters will be estimated from *in vitro* measurements.

The model has five variables. Four of them are presynaptic firing rates. To investigate their differential contribution, the proximal and distal parts of the dendritic trees have been separated and each of them has two presynaptic rates corresponding to the excitatory and inhibitory populations (hence four rate variables: ν_e^p, ν_i^p, ν_e^d, ν_i^d). Additionally, a global synchrony variable has been introduced for presynaptic events. This reproduces the effect of pairwise correlations observed in neocortical assemblies (Peyrache et al., 2012) and/or the multi-innervation of a cell by its presynaptic afferent *ref-multi-innervation*. The synchrony degree in the presynaptic activity has been suggested to vary with stimulus statistics in the primary visual cortex (Baudot et al., 2013; El Boustani and Destexhe, 2009) and justifies its introduction as a variable.

III.3 Model calibration on *in vitro* measurements

We will use the firing response function of our companion study, we therefore wanted a characterization of the passive and morphological properties on the same experimental system: layer V pyramidal neurons in the primary visual cortex of young mice. To this purpose, we performed measurements of the input impedance at the soma with intracellular recordings *in vitro* in n=13 cells. The
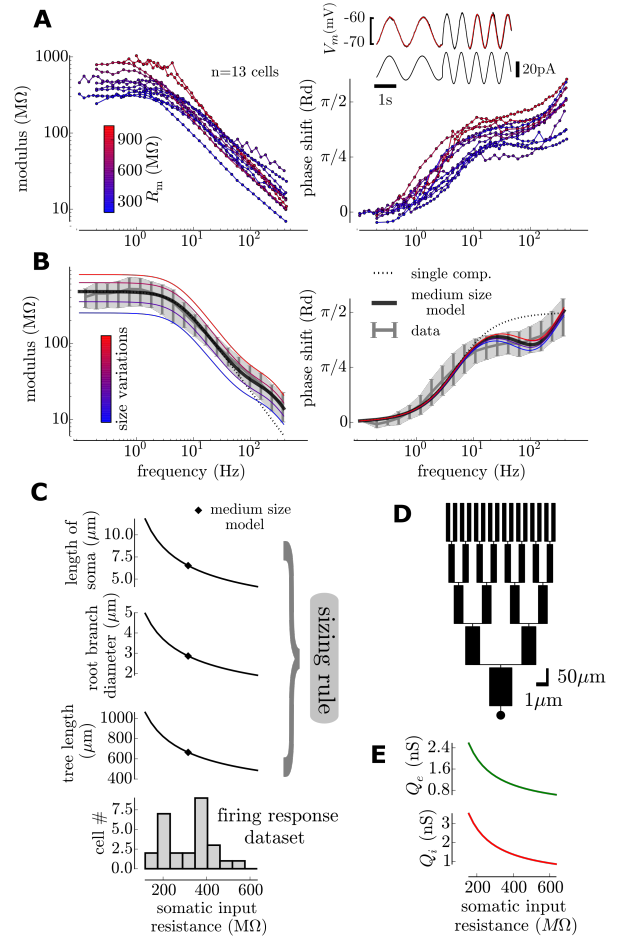
Figure 2: **Calibrating the model on *in vitro* measurements: the simplified model and its size variations provides an approximation for the somatic input impedance and its heterogeneity**. **(A)** Input impedance (left: modulus and right: phase shift) measured at the soma in intracellular recordings with sine-wave protocols in current-clamp (inset). The color code indicates the input resistance and is likely to result from size variations of individual cells. **(B)** A medium size model accounts for the average data and varying the size of the dendritic tree and soma reproduces the trend in the individual measurements. Large cells (blue) have a lower modulus and a lower phase shift while small cells (red) have both a higher modulus and phase shift. **(C)** We obtain a map between input resistance and size of the morphological model. **(D)** Representation of the medium-size model. **(E)** Additionally the synaptic weights are rescaled with respect to the cell's somatic input resistance. Because the mean transfer resistance to soma is linked to the input resistance, this rescalings insures that the mean synaptic efficacy at soms is the same for all cells.

key property on which this characterization relies is the fact that the input impedance at the soma can not be accounted for only by the isopotential somatic compartment (i.e. a RC circuit). The input impedance also shows the contribution of the dendritic tree in parallel to the soma (see (Rall, 1962) for the classical description on the *xx*

motoneuron). Indeed, both the modulus and the phase of the imput impedance show deviations from the deviations from the RC circuit impedance (see the comparison in Figure 2B): see for example the exponent of the power law scaling of the modulus (-1 for the single compartment and ~ 0.7 for pyramidal cells) or the decreased phase shift at 100Hz.

We first average all data (shown on Figure 2A) to obtain a mean input impedance (shown on Figure 2B) representative of a mean cellular behavior. We then perfomed a minimization procedure to obtain both the passive properties and the morphology corresponding to this average behavior (see Methods V.9). The obtained passive properties were compatible with standard values, e.g. the resulting specific capacitance was 1.05 $\mu F/cm^2$ close to the 1 $\mu F/cm^2$ standard, thus suggesting that the procedure could capture the physiological parameters of pyramidal cells, see Table 1 for the other parameters. Also the obtained morphology seems realistic (B=5 generation of branches, a total tree length of L_t=*xx* μ m and a root branch diameter of the tree D_t = *xx* μ m) given what can be observed after histological work (Zerlaut et al., 2016). Most importantly, the surface area was physiologically realistic, so that when using synaptic densities, we obtain an accurate number of synapses. A representation of this mean morphology can be seen on Figure 2D.

Pyramidal cells show a great variablity in input impedance, for example their input resistance almost spans one order of magnitude (both in the present n=13 cells, see the low frequency modulus values in Figure 2A, as well as in the firing response dataset, see bottom in Figure 2C). We found that varying the size of the morphological model within a given range around the mean morphological model could partially reproduce the observed variability in the input impedance profiles (see Figure 2B). Size variations corresponds to a linear comodulation of the 1) tree length L_t, 2) the diameter of the root branch D_t and 3) the length of the somatic compartment L_S (see Figure 2C for the range of their variations). On Figure 2A, the cells have been colored as a function of their input resistance while on Figure 2B, we vary the size of the size of the morphological model. Large cells (blue, low input resistance) tend to have a lower input resistance and phase shift than the small cells (red, high input resistance). Note that thais very simplistic account of morphological variations only very partially describes the observed behavior in pyramidal cells. In particular, it strongly underestimates the variations of phase shifts at medium and high frequencies (f>20Hz). This discrepancy is likely to be due to the details of dendritic arborescence that are not captured by the strong constraints of our dendritic model (symmetric branching, diameter rules, number of branches, etc...). Despite those discrepancies, size variations in our morphological model constitute a reasonable first approximation to account for cellular variety within the layer V pyramidal cell population.

This characterization, combined with the analytical tractability of the model (see *sec:sec:Zin-measure*) allow us to construct a map between input resistance at the soma and size of the morphological model (the passive properties
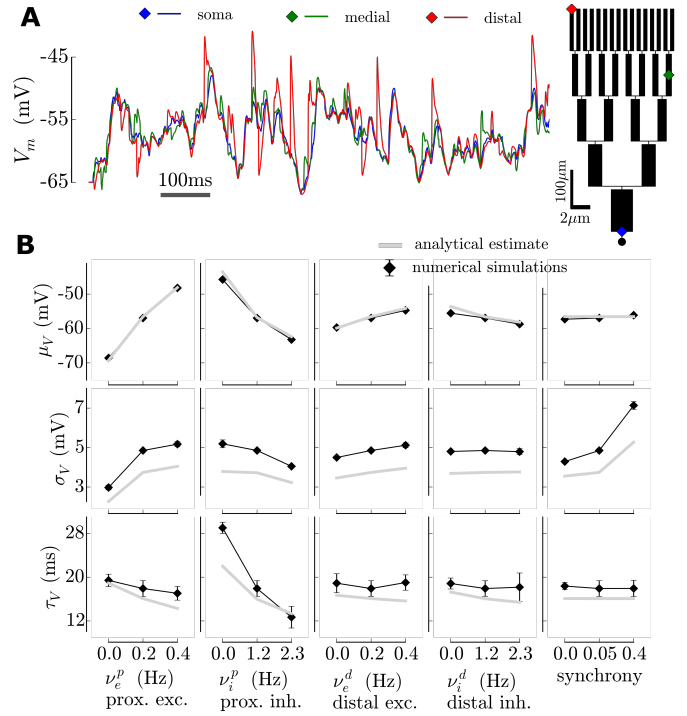
Figure 3: Accuracy of the analytical estimate for the properties of the membrane potential fluctuations at the soma: comparison between numerical simulations and the analytical approximation. Shown for the medium size model of Figure 2D. **(A)** In the numerical simulation, we explicitly simulate the whole dendritic arborization, we show the membrane potential variations for the three locations shown on the left. **(B)** Properties of the membrane potential fluctuations for different configuration of presynaptic activity: analytical predictions and output from numerical simulations in NEURON. In each column, one variable is varied while the other variables are fixed to the mean configuration value corresponding to $\nu_e^p = \nu_e^d = 0.2$Hz, $\nu_i^p = \nu_i^d = 1.2$Hz and s=0.05.

are set as identical, the one fitted on the mean impedance behavior). Thus, for each neuron in our previous "firing response dataset", because we have its input resistance at the soma, we can associate a given morphology. The association rule is shown in Figure 2C.

Mean number of synapses: 3953 ± 1748 with a ratio of excitatory to inhibitory numebers of synapses of 4.5 ± 0.1.

III.4 An analytical approximation for the properties of the membrane potential fluctuations at the soma

For each cell, we now want to translate the five variables of the model in terms of membrane potential fluctuations properties at the soma (μ_V, σ_V, τ_V) on which we will apply the cell's firing response function. To obtain a final map between the input (the five model variables) and the output (the spiking probability).

Investigating dendritic integration for detailed morphological structures is made difficult by the fact that this has to be done numerically with a relatively high spatial and

temporal discretization. In the fluctuation-driven regime, one also needs to sample over long times (T ≫ τ_V ~ 10ms) to obtain the statistical properties of the somatic V_m resulting from dendritic integration. In addition, we have n=27 different morphologies in this study and we will explore a five dimensional parameter space (the five variable of our model). Under those conditions, if performed numerically, the computational cost of such a study is clearly prohibitive. We briefly describe here, why, in our simplified model, an analytical treatment is nonetheless possible and thus render this investigation feasible (see details in the Methods V.5 and in the Supplementary Material). The key ingredient is the ability to reduce the dendritic tree to an equivalent cylinder (Rall, 1962), we only adapted this reduction to the changes in membrane permeability associated to the high conductance state (Destexhe et al., 2003). Two approximations underlie our estimation: 1) the driving force during an individual synaptic event is fixed to the level resulting from the mean bombardment (Kuhn et al., 2004) and 2) the effect at the soma of an synaptic event at a distance x in a branch of generation b, corresponds to $1/2^{b-1}$ the post-synaptic response to the stimulation made of synchronous events at distance x in all the 2^{b-1} branches of the generation b. Luckily, the combination of those approximation is a favorable situation. Indeed, hypothesis 1) overestimates the size of post-synaptic events (because the driving force is not fixed, it diminishes during the PSP time course) while hypothesis 2) underestimates the size of post-synaptic events (because of the $2^{b-1}-1$ synchronous events in neighboring branches, the membrane conductance is higher than in the case of a single event, consequently neighboring events have a shunting effect that artificially descreases the response). In addition, both of those approximation are likely to hold when single events are of low amplitude compared to the amplitude of the massive synaptic bombardment (see e.g. Kuhn et al. (2004) for the validity of the first hypothesis).

In Figure 3, we compare the analytical approximation to the output of numerical simulations performed with the `NEURON` software (Hines and Carnevale, 1997). We varied the five variables of the model around a mean synaptic bombardment configuration (see next section). Some discrepancies between the approximation and the simulations appeared, in particular one can see a ~ 1mV shift in the standard deviation σ_V of the fluctuation. Because the synchrony controls the amplitude of the fluctuations (Figure 3B and Figure 4B), the analytical estimate could therefore be seen as an accurate estimate, modulo a shift in the synchrony. Nonetheless, the trend in the variations of the fluctuations as a function of the model variables is globally kept between the analytical estimate and the numerical simulations. This relatively good agreement therefore shows that our analytical estimate is a valid tool to study dendritic integration in the fluctuation-driven regime.
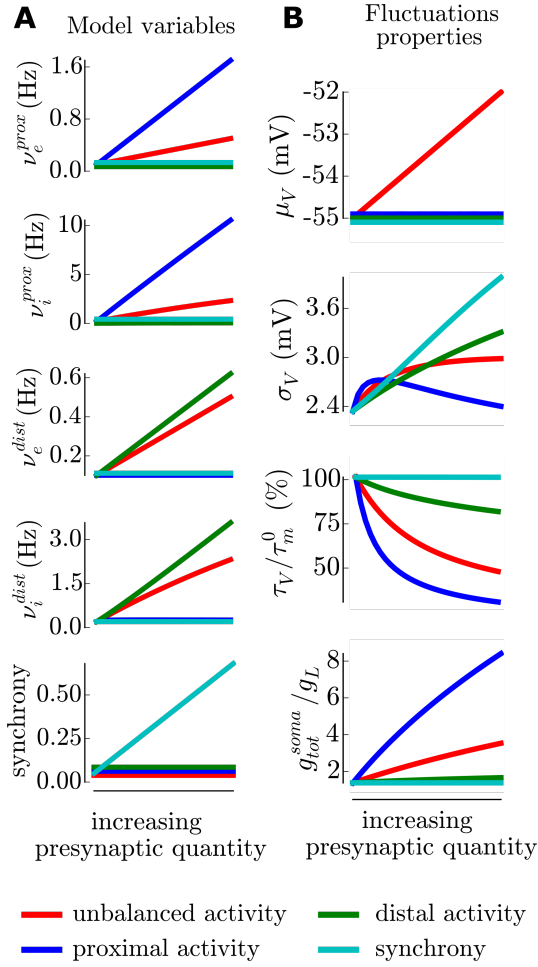
III.5 Properties of the fluctuations for different types of presynaptic activity

We now implement various types of presynaptic activity and investigate the properties of the resulting membrane potential fluctuations at the soma. In addition, we represent the variations of the somatic input conductance (relative to the leak input conductance) because, as it is routinely measured in intracellular studies *in vivo*, this quantity allows a comparison between the model and experimentally observed activity levels. On Figure 4, we present those different protocols, on the left one can see how the five variables of the model are comodulated for each protocol (color coded, see bottom legend) and one the left, one can see the resulting properties of the membrane potential fluctuations. We present those results only for the medium-size model, but it was calculated for the morphologies associated to all cells. The variability introduced by the various morphologies is studied in the Supplementary Material and we found that the qualitative behavior discussed in this section was preserved in all cells.

We first introduce a baseline level of presynaptic activity corresponding to a low level of network activity: g_{tot}^{soma}/g_L ~ 1.7, compared to ~ 3-4 in activated states, reviewed in Destexhe et al. (2003). This baseline activity is a mix of proximal and distal activity with a low degree of synchrony (s=0.05). Similarly to (Kuhn et al., 2004), the inhibitory activity is adjusted to obtain a balance of the V_m fluctuations at -55mV. The firing values of this baseline level are very low ($\nu_e^d = \nu_e^p = xx$ for the excitation and $\nu_i^d = \nu_i^p = xx$ for the inhibition) in accordance with the sparse activity characterizing mammalian neocortical dynamics *refs*. On top of this non-specific background activity, we will now add a specific stimulation.

We start with unbalanced activity. We define it as a stimulation that brings the mean membrane potential above -55mV corresponding to the previously defined balance. The stimulation corresponds to an increase of the excitatory synaptic activity (still running within a very sparse range of activity, $\nu_e^d = \nu_e^p \in [0.05, 0.5]$Hz) with an increasing inhibitory activity adjusted to linearly disrupt nthe balance between -55mV and -52mV (see Figure 4). The synchrony is kept constant and the activity indifferentially raises in the proximal and distal part. This increase of total activity raises the input conductance ratio close to four. In this moderate range, the variations of the amplitude of the fluctuations σ_V remains a monotonic increase (unlike the non-monotonic variations found in the single-compartment study of Kuhn et al. (2004) and the case of a proximal stimulation, see below), the fluctuations gets approximately twice faster (the normalized autocorrelation time τ_V/τ_m^0 decays from 100% to 50%) and, of course (by design), the mean depolarization has a linear increase of 3mV.

We now emulate purely proximal activity. To this purpose, we fix the distal presynaptic firing frequencies (ν_e^d and ν_i^d) as well as the synchrony to their baseline levels. To remain in a sparse activity level, we increase the proximal excitatory activity from the baseline level to 1.7Hz and we adjust proximal and somatic inhibitory activity to keep the

A Model variables **B** Fluctuations properties

Figure 4: Properties of the membrane potential fluctuations for different types of presynaptic activity: either unbalanced, purely proximal, purely distal, synchronized (color code). A common baseline configuration of low balanced proximal and distal activity gives rise to baseline fluctuations properties, then we increase a given type of activity. **(A)** Model variables to achieve varying levels of those different types of activity. **(B)** Membrane potential fluctuations properties and somatic input conductance at the soma for the different protocols. Shown for the medium-size model, see Supplementary Material for the variability introduced by variations in cell morphologies.

balance at the soma. This would nonethless correspond to large network activity level, as can be seen from the input conductance ratio (that raises up to 8). This situation gives results comparable to the single-compartment study of Kuhn et al. (2004). The amplitude of the fluctuations has a non-monotonic profile and the autocorrelation time strongly decreases. A notable difference is that, even if we investigated high activity levels, the autocorrelation time does not goes to zero and the amplitude of the fluctuations has only a moderate decrease. This discrepancy is due to 1) the choice of non-negligible synaptic time constants compared to the membrane time constants (here τ_{syn}=5ms and $\tau_m^0 \sim$ 25ms, then τ_V/tau_m^0 would saturate at $\tau_{\text{syn}}/\text{tau}_m^0 = 20\%$) and 2) the fact that the synaptic input is distributed attenuates the strong shunting effects

observed in the single compartment case.

For distal activity, we keep the proximal presynaptic frequencies (ν_e^{p} and ν_i^{p}) as well as the synchrony to their baseline levels. We increase the distal excitatory activity from the baseline level to a moderate level: 0.7Hz. The distal inhibitory frequency is again adjusted to keep the balance at the soma. Here, we get a different picture than in the proximal case, the increase in activity leads to negligible increase of the somatic input conductance as expected from electrotonically distant input (**?**). Also, the decrease of the speed of the fluctuations is much attenuated, the reason for this is that only the distal part has a high conductance, consequently post-synaptic events are strongly low-pass filtered by the proximal part of the arborization before reaching the soma. Here, the amplitude of the fluctuations strongly increases as a function of the input and do not show the non-monotonic relation found for proximal input. This is explain by the combination of the fact that 1) distal events are of higher amplitude and 2) the shunting of post-synaptic events is much reduced due to the relatively narrow localization of the synaptic conductances.

Finally, we emulate an increase in the presynaptic synchrony. Here, all synaptic frequencies are kept constant with respect to the baseline level and we simply increase the probability of coincident events for each synaptic spike train. Because there is no change in synaptic activity, this stimulation does not affect the input conductance ratio, neither the mean membrane potential or the speed of the fluctuations. However, presynaptic synchrony strongly affects the amplitude of the fluctuations in a near linear manner.

Note, that in addition to the sparse activity constraints or the balance constraints, the criteria for the ranges of the model variables was manually choosen to have the fluctuations in the same domain. For example, we investigated a lower activity range for the distal part than for the proximal part to avoid an explosion of σ_{V}, the range for the synchrony increase follow the same criteria.

We thus demonstrated here, that, in a theoretical model of dendritic integration, the properties of the fluctuations (μ_{V}, σ_{V}, τ_{V}) can follow various comodulations, depending on the properties of the synaptic stimulation. This behavior is what motivated to fully scan the three dimensional space (μ_{V}, σ_{V}, τ_{V}) in our companion study and not only one comodulation type, see Rauch et al. (2003) as an example *find better*, it would correspond to the single-compartment approximation with current-based synapses .

III.6 Heterogeneous firing responses induce diverse coupling to presynaptic activity

For each one of the n=27 cells of our companion study (Zerlaut et al., 2016), we now have 1) a morphological model and 2) a firing response function $\nu_{out} = \mathcal{F}(\mu_V, \sigma_V, \tau_V)$. Thanks to the analytical approximation, we can translate the five model variables ($\nu_e^p, \nu_i^p, \nu_e^d, \nu_i^d, s$) into the stationary fluctuations properties (μ_V, σ_V, τ_V) that, in turn, the
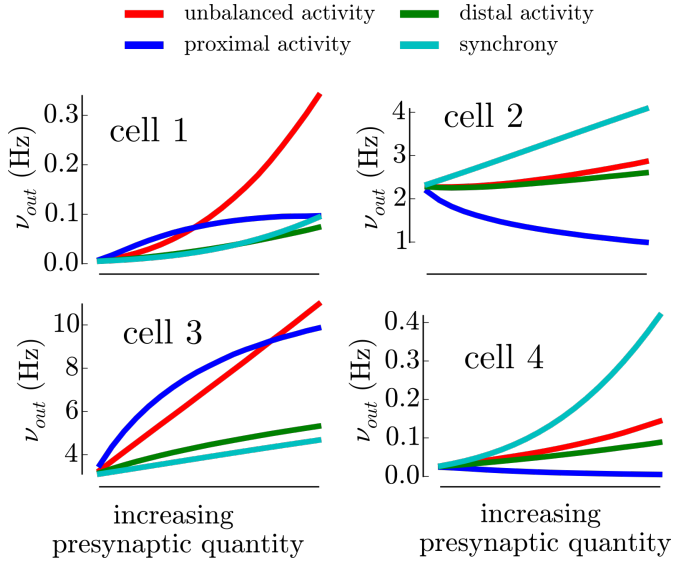
Figure 5: Examples of the firing response of 4 different cells for the different synaptic inputs (color-coded) shown in Figure 4. The abcissa corresponds to the variations of the model variables shown in Figure 4A

firing response trsanslate into a spiking probability. Thus, we finally get the full *input-output* function (within our theoretical framework) as illustrated on Figure 1A.

We show on Figure 5 the response of four cells to the different types of presynaptic activity described in the previous section. The responses show qualitative and quantitative differences, we briefly discuss them here and we perform a more rigorous analysis in the next section.

First, we can see that individual cells have a very different level of response to the baseline level of synaptic activity (initial response in Figure 5). Cell 1 has a baseline at $\sim 10^{-2}$ Hz while Cell2 or Cell3 have response above 1Hz, i.e. two orders of magnitude above.

Importantly, those cells have different preferences for particular types of stimulations. Cell 1 responds more to unbalanced activity whereas Cell 2 and Cell 4 respond more to an increase in synchrony and Cell 3 responds preferentially to proximal activity (within this range). This is what we mean by *preferential coupling*: individual neurons will respond preferentially to a particular type of synaptic activity. An even more pronounced discrepancy appears for proximal activity: the response can be either increased (Cell 1 and Cell 3) or decreased (Cell 2 and Cell 4) with respect to the baseline level.

Given the relative invariance of the fluctuations properties for each cell (see previous section, despite the various morphologies, the same input creates the same fluctuations), those differences are the consequences of the heterogeneity in the firing responses, we conclude that *heterogeneous firing responses induce diverse coupling to presynaptic activity.*

## III.7 Biophysical origin of the heterogenous couplings to presynaptic activities

We now make this analysis more quantitative by computing the responses for all n=27 cells. We get their response to the baseline level ν_{bsl} and their mean response change for each stimulation type (the mean over the range of scanned presynaptic input): $\delta\nu_{\mathrm{ubl}}$ for the unbalanced activity, $\delta\nu_{\mathrm{prox}}$ for the proximal activity, $\delta\nu_{\mathrm{dist}}$ for the distal activity and $\delta\nu_{\mathrm{synch}}$ for an increased sychrony. We show the histogram of those values in the left column of Figure 6. We also look for the origin of the individual couplings by correlating them with the characteristics of the neuronal firing responses (Zerlaut et al., 2016).

We first analyze the response to baseline activity ν_{bsl}. When log-scaled (Figure 6A), the distribution is approximately normal and spans 2-3 orders of magnitude. This log-normal distribution of pyramidal cell firing rates during spontaneous activity seems to be a hallmark of mammalian neocortical dynamics (see e.g. *Peyrache* in human neocortex). We investigated what properties of the firing responses could explain this behavior, we therefore looked for correlations between our measures of the firing responses in the fluctuation-driven regime (Zerlaut et al., 2016) and the baseline responses. Not surprisingly, we found a very strong linear correlation between the excitability $\langle V_{\mathrm{thre}}^{\mathrm{eff}}\rangle_{\mathrm{D}}$ and the baseline response level, the other characteristics semt to have no impact (Pearson correlations, see values in Figure 6A). Again, it should be stressed that presynaptic connections are non-specific, those results therefore show that the typical log-normal distribution of firing rates could very naturally emerge as a result of the normal distribution observed in pyramidal cell's excitabilities (Zerlaut et al., 2016), thus suggesting that no specific circuitry is needed to explain this neocortical property.

Despite the important differences in the fluctuations they create (see Figure 4B), the responses over cells to unbalanced activity, distal activity and an increased synchrony share a very similar behavior. Their firing increases show a strong heterogeneity over cells, covering two orders of magnitude (see log y-axis on Figure 6B,D,E). This variability in responses was again highly correlated with the excitability. Surprisingly, the response was not dependent on any other of the characteristics of the firing response. For example, the variability observed during an increase in synchrony could have been linked to the to the sensitivity to the standard deviation σ_V $\langle\partial\nu/\partial\sigma_V\rangle_{\mathcal{D}}$, but this effect was not significant (p>0.05, Pearson correlation). This analysis therefore revealed that, for those type of synaptic activities, those properties of the firing response have negligible impact compared to the very strong effect of the variability in excitabilities. In the Supplementary Material we also investigated whether, after accounting for the variability due to the excitability, the residual variability would be explained by the characteristics of the firing response. Again, correlations were not significant, suggesting that those quantities have a very low explanatory power on the firing responses for those types of stimuli.

The response to proximal activity also showed a great variability but with a qualitatively different behavior (Fig-
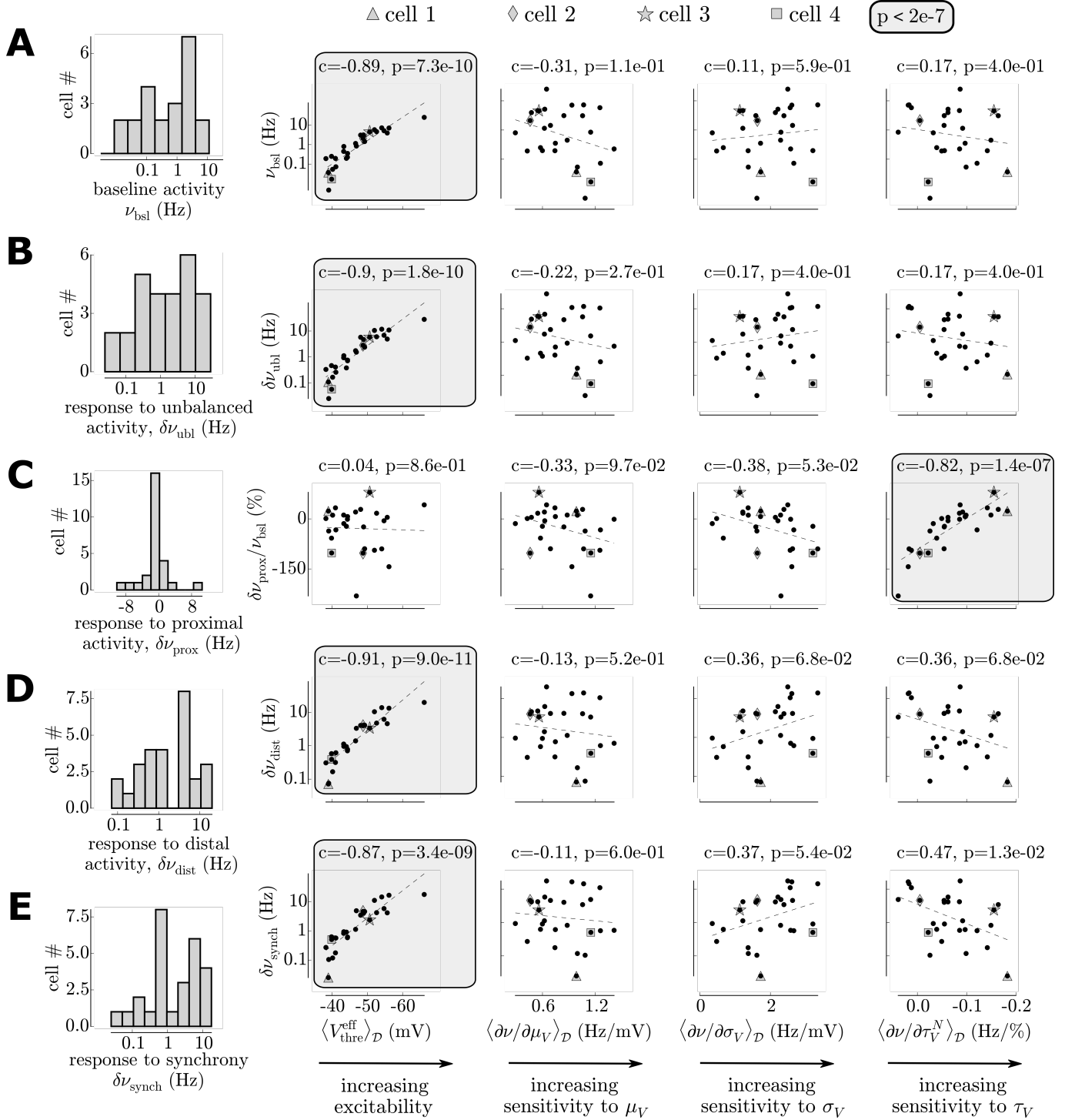
Figure 6: Diverse cellular responses to synaptic stimulation and their link to the chracteristics of their firing response function. Note the logarithmic scale for the firing respones in **B,C,D**. **(A)** Diverse response to baseline stimulation. **(B)** Diverse response to unbalanced activity. **(C)** Diverse response to proximal activity. Note that because the response also show negative changes of firing rate, the data can not be log-scaled. Instead, they have been rescaled by the baseline response. **(D)** Diverse response to distal activity. **(E)** Diverse response to a synchrony increase.

ure 6C). Notably, firing could be suppressed or increased. This variability was independent of the excitability of the cells but was correlated with the sensitivity to the speed of the fluctuations $\langle \partial \nu / \partial \tau_V^N \rangle_{\mathcal{D}}$. Indeed, the proximal stimulation implies a strong variations of the fluctuations speed (i.e. decreasing τ_V, while keeping moderate variations of σ_V and, by design, a constant μ_V) thus rendering the sensitivity to the fluctuation speed the critical quantity for this stimulation type.

IV   Discussion

IV.1   Sum up

In this communication, we investigated how the heterogeneity in firing responses to fluctuating input shape the diverse input-output functions of neocortical pyramidal cells. Focusing on the regime of near asynchronous population dynamics, we emulated various type of presynaptic activity in a theoretical model of dendritic integration. We found that those different types of synaptic stimulation corresponds to various comodulations of the fluctuations properties, and that, because of their different response to the same fluctuations, individual neurons would respond differently to those stimulation.

- Note that proximal activity in our theoretical model has a rather large extent, six seventh of the dendritic tree belongs to the proximal part.

IV.2   Limitations of the proposed theoretical framework for single-cell computation

- Only enables to scan sensory processing

- no active mechanisms in dendrites !!

IV.3   Relevant functional measures of cellular properties in the fluctuation-driven

Very naturally, a key quantity to explain the various neuronal responses was the cellular excitability. Indeed, the response to unbalanced activity, distal activity or an increase in synchrony was strongly correlated with cellular excitability. Also the sensitivity to the speed of the fluctuations had a crucial impact on the response to proximal activity.

The present analysis therefore shed light on the physiological relevance of the properties that we introduced in our companion study.

Therefore, in all four measures characterizing the cellular properties in the fluctuation-driven regime that we introduced in our companion study, only two of them seems to be physiologically relevant: the excitability and the sensitivity to the speed of the fluctuations.

We showed here that to of them seems irrelevant and do not have any explanatory power . A significant heterogeneity was found for those two quantities in between

cells, but when plugged in a physiological situation, those quantities

To highlight the impact of the *biophysical specificity*, we investigated single neuron response in a framework where the *circuit specificity* was null (all neurons had the same afferent connections)

- By introducing an analytically tractable dendritic model, we presented

the final form of our theoretical framework for single cell computation in the fluctuation-driven regime.

- We used a second dataset to characterize the morphology, so that we could do it on the "firing response dataset"

IV.4   An analytical model for dendritic integration in the fluctuation-driven regime

- we provided a stratey for the analytical treatment of dendritic integration in the fluctuation-driven regime that relies on 1) shotnoise theory, 2) cable theory and 3) adequate approximations.

- The main advantage of this model is that you can very naturall plug in physiological parameters (because surface area is physiological as well as transfer resistance to soma) and still it remains analytical.

- Literature suffers from the reduction to single-compartment. Though being approximative.

- The current model provides a tool to make network dynamics question amenable to mathematical analysisw ith morphologically detailed models.

- Rely on calculating PSP events and opens the way toward event based simulations of dendritic integration in the high conductance state (though including approximation).

IV.5   Heterogeneity of morpological and passive neuronal properties

In this study, the rescaling rule between input resistance at the soma and the size of the morphological model has led to the invariance in the relation between input (presynaptic variables) and the fluctuation properties. Thus the heterogeneity in morpholgies (here only cell sizes) had very little effects on the heterogeneity of cell responses. Nontheless

IV.6   Diverse coupling to proximal activity and *in vivo* observations

The *in vivo* study in mice visual cortex of Okun et al. (2015) reported a strong heterogeneity in the coupling between individual cell's responses and the locally recorded population activity. The authors explained those observations by a variabiliy in the local recurrent connectivity and argued that this diverse coupling did not seem to be explained

by biophysical heterogeneity (e.g. the coupling was independent from the action potential threshold, somehow a measure of the excitability). However, as local connectivity is thought to target more proximal regions (Spruston, 2008), our study proposes a biophysical mechanism that could contribute to their observation. The diverse coupling to proximal activity was indeed found to be independent on the cellular excitability (see Figure 6), the critical quantity to explain this feature was the sensitivity to the speed of the fluctuations. Note that two strong hypothesis underlie the previous reasoning: 1) that local population activity correspond to the proximal activity modeled our study, i.e. the activity should remains balanced, elicits strong changes in the speed of the fluctuations while limiting variations of σ_V and 2) that the biophysical heterogeneity for the sensitivity to τ_V observed in young mice cortex is at least partially preserved in adult animals. Future work could therefore adress this question by combining recordings of population activity with a more subtle and functionnally-relevant analysis of single cell properties.

IV.7 Sodium inactivation and sensitivities to τ_V

In our companion communication, theoretical modeling suggested that the sensitivity to the speed of the fluctuations to the impact of sodium inactivation and the density of sodium channels

V Material and Methods

V.1 Morphological model

The morphology of our theoretical model is the following (depicted in Figure 1B): it is made of an isopotential somatic compartment (i.e. a leaky RC circuit) in parallel with a dendritic structure. The dendritic tree is an arborization of total length L_t containing B generation of branches. For simplicity all branches of a generation $b \in [1, B]$ have a length L_t/B. From one generation to the other, a branch divides into two branches where the diameter of the daughter branches follows Rall's 3/2 branching rule (Rall, 1962): $(d_{b+1})^{\frac{3}{2}} = (d_b)^{\frac{3}{2}}/2$, i.e. $d_b = 2^{-\frac{2}{3}} d_t \setminus$) where d_t in the diameter of the root branch of the dendritic tree.

The parameters of the model are presented on Table 1.

V.2 Model equations: synaptic input and passive properties

The cable equation describes the temporal evolution and spatial spread of the membrane potential along the branches of the dendritic tree (Rall, 1962):

$$\frac{1}{r_i}\frac{\partial^2 v}{\partial x^2} = i_m(v, x, t) = c_m \frac{\partial v}{\partial t} + \frac{v - E_L}{r_m} - i_{syn}(v, x, t) \quad (1)$$

the membrane current $i_m(v, x, t)$ is a linear density of current (the presented cable equation already includes the radial symmetry). Though the modeled system has several branches, the equation can be written as a single spatial dependency x because the symmetry of the model across branches imply that

the properties of the input are identical at a given distance to the soma.

Synaptic input is modeled by local (infinitely small) and transient changes of membrane permeability to selective ionic channels. Both excitatory (accounting for AMPA synapses) and inhibitory synapses (accounting for GABAa synapses) are considered, their reversal potential is E_e=0mV and E_i=-80mV respectively. Each synaptic event is generated by a shotnoise and its effect on the conductance is a jump followed by an exponential decay. The form of the synaptic current is therefore:

$$\begin{cases} i_{syn}(v, x, t) = g_e(x, t)(E_e - v) + g_i(x, t)(E_i - v) \\ g_e(x, t) = \sum_{\{x_e, \{t_e\}\}} \delta(x - x_e) \sum_{t_e} \mathcal{H}(t - t_e) Q_e(x) e^{-\frac{t - t_e}{\tau_e(x)}} \\ g_i(x, t) = \sum_{\{x_i, \{t_i\}\}} \delta(x - x_i) \sum_{t_i} \mathcal{H}(t - t_i) Q_i(x) e^{-\frac{t - t_i}{\tau_i(x)}} \end{cases}$$

$$(2)$$

where g_e and g_i are linear densities of conductances. Each synapse, indexed by s, has a position x_s and a set of presynaptic events $\{t_s\}$, hence the iteration over $\{x_s, \{t_s\}\}$ for the sum over synapses for each synaptic type. $\mathcal{H}$ is the Heaviside step function. The presynaptic events $\{t_s\}$ are generated by point processes at fixed frequencies ν_s with a given degree of synchrony, see details in the next section V.3.

The model distinguishes two domains : a proximal domain with the upper index p and a distal domain with the upper index d (see Figure 1). Then the space-dependent quantities (presynaptic frequencies, synaptic quantal and synaptic decay time constant) can be written as :

$$\begin{cases} \nu_e(x) = \nu_e^P + (\nu_e^d - \nu_e^p)\mathcal{H}(x - l_p) \\ \nu_i(x) = \nu_i^P + (\nu_i^d - \nu_i^p)\mathcal{H}(x - l_p) \\ Q_e(x) = Q_e^P + (Q_e^d - Q_e^p)\mathcal{H}(x - l_p) \\ Q_i(x) = Q_i^P + (Q_i^d - Q_i^p)\mathcal{H}(x - l_p) \\ \tau_e(x) = \tau_e^P + (\tau_e^d - \tau_e^p)\mathcal{H}(x - l_p) \\ \tau_i(x) = \tau_i^P + (\tau_i^d - \tau_i^p)\mathcal{H}(x - l_p) \end{cases}$$

$$(3)$$

The continuity of the membrane potential and of the current at the boundaries between the proximal and distal part imply:

$$\begin{cases} v(l_p^-, t) = v(l_p^+, t) \\ \frac{1}{r_i}\frac{\partial v}{\partial x}\Big|_{l_p^-} = \frac{1}{r_i}\frac{\partial v}{\partial x}\Big|_{l_p^+} \end{cases}$$

$$(4)$$

where the limit with upper index $\pm$ indicate the limit taken from the left or the right respectively.

At the soma, $(x = 0)$, we have a lumped impedance compartment. It has leaky RC circuit properties and also receives synaptic inhibition, the somatic membrane potential therefore follows :

$$\begin{cases} C_M \frac{dV}{dt} + \frac{V - E_L}{R_M} + G_I(t)(V - E_i) + I(t) = 0 \\ G_i(t) = \sum_{N_i} \sum_{\{t_i\}} Q_i^p e^{-\frac{-(t - t_i)}{\tau_i^p}} \mathcal{H}(t - t_i) \end{cases}$$

$$(5)$$

where $I(t)$ is the time-dependent input current from the soma into the dendrite. R_M and C_M are the RC properties of the lumped compartment (capital letters will indicate the somatic properties throughout the calculus). N_i is the number

Table 1: Model parameters. The passive properties and the mean morphology are fitted while

Parameters	Parameter Name	Symbol	Value	Unit
passive				
	leak resistivity density	r_m	325	μS/cm^2
	intracellular resistivity	r_i	30	Ω .cm
	specific capacitance	c_m	1.05	μF/cm^2
	leak reversal potential	E$_L$	-65	mV
synaptic				
	inhibitory reversal potential	E$_i$	-80	mV
	excitatory reversal potential	E$_e$	0	mV
	somatic excitatory density	$\mathcal{D}_e^{soma}$	0	synapses/$(100\mu m^2)$
	somatic inhibitory density	$\mathcal{D}_i^{soma}$	20	synapses/$(100\mu m^2)$
	tree excitatory density	$\mathcal{D}_e^{tree}$	30	synapses/$(100\mu m^2)$
	tree inhibitory density	$\mathcal{D}_i^{tree}$	6	synapses/$(100\mu m^2)$
	prox. excitatory weight	Q$_e^{0,p}$	0.7	nS
	prox. inhibitory weight	Q$_i^{0,p}$	1.	nS
	distal excitatory weight	Q$_e^{0,d}$	1.05	nS
	distal inhibitory weight	Q$_i^{0,d}$	1.5	nS
	excitatory decay	τ_e	5	ms
	inhibitory decay	τ_i	5	ms
Mean morphology				
	soma length	L$_S$	5.0	μm
	soma diameter	D$_S$	15.0	μm
	root branch diameter	D$_t$	2.25	μm
	tree length	L$_t$	550.0	μm
	branch number	B	5	
	Proximal tree fraction	f$_{prox}$	7/8	

of somatic synapses, each of them generates a point process $\{t_i\}$ of inhibitory synaptic events. The properties of the somatic synapses (ν_i^S, Q_i^S) are equivalent to the proximal ones.

This equation with the membrane potential continuity will determine the boundary condition at the soma (x=0). We identify $V(t) = v(0,t)$, then $I(t)$ is the current input into the dendritic tree at $x = 0$ so it verifies:

$$\frac{\partial v}{\partial x}_{|x=0} = -r_i\, I(t) \qquad (6)$$

So:

$$\frac{\partial v}{\partial x}_{|x=0} = r_i \left(C_M \frac{\partial v}{\partial t}_{|x=0} + \frac{v(0,t) - E_L}{R_m} + G_I(t)\,(v(0,t) - E_i) \right) \qquad (7)$$

Finally, the last boundary condition is that all branches terminate with an infinite resistance that impede current flow (sealed-end boundary conditions):

$$\frac{\partial v}{\partial x}_{x=l} = 0 \qquad (8)$$

Together with the biased Poisson process for event generation (see the next section V.3), the final set of equations that describes the model, is therefore:

$$\begin{cases} \frac{1}{r_i}\frac{\partial^2 v}{\partial x^2} = c_m \frac{\partial v}{\partial t} + \frac{v - E_L}{r_m} - i_{syn}(v,x,t) \\ \frac{\partial v}{\partial x}_{|x=0} = r_i \left(C_M \frac{\partial v}{\partial t}_{|x=0} + \right. \\ \qquad \left. \frac{v(0,t) - E_L}{R_m} + G_I(t)\,(v(0,t) - E_i) \right) \\ v(l_p^-, t) = v(l_p^+, t) \\ \frac{\partial v}{\partial x}_{l_p^-} = \frac{\partial v}{\partial x}_{l_p^+} \\ \frac{\partial v}{\partial x}_{x=l} = 0 \end{cases} \qquad (9)$$

V.3 Model of presynaptic activity

Presynaptic activity is modelled as a discrete set of presynaptic events. Because of the apparent random spiking activity in the fluctuation-driven regime, the basis for the generation of those discrete events is the Poisson process. Nonetheless, we want to reproduce the additional degree of presynaptic synchrony found in neocortical asssemblies that result mainly for two phenomena: 1) pairwise correlation between neurons *refs* and 2) muti-innervation of a cell by a presynaptic neuron *refs*. We therefore introduce a variable s that will bias the event generation of the Poisson process ($s \in [0, 1]$). For simplicity in the analytical treatment, synchrony in presynaptic activity is not shared across different synapses. We arbitrarily limit the number of coincident events to four events, therefore for a degree of synchrony s: single events have a probability $1 - s$, double events have a probability $s - s^2$, triple events events have a probability $s^2 - s^3$ and quadruple events have a probability

s^3. To generate a biased Poisson process of frequency ν with a degree of synchrony s, we therefore generate a Poisson process of frequency:

$$\nu_{synch} = \frac{\nu}{1 + s + s^2 + s^3} \qquad (10)$$

and we duplicate (from up to four events) each event according to their probabilities of occurence.

This is a very simplistic and limited model of presynaptic synchrony but it is sufficient for reproducing the impact of synchrony on the quantities investigated in this paper (only the variance of the membrane potential fluctuations).

V.4 Numerical implementation

The full model has been implemented numerically using the `NEURON` software. The branched morhology was created and passive cable properties were introduced (see Table 1). The spatial discretization was `nseg=30` segments per branch. On each segment, one excitatory and one inhibitory synapse were created, the shotnoise

frequency was then scaled according to the segment area and the synaptic density to account for the number of synapses on this segment (using the properties of the Poisson process, N synapses at frequency ν is a synapse at frequency $N\nu$). Custom event generation was implemented to introduce correlations (instead of classical `NetStim`) and fed `NetCon` objects attached to each synapses (`ExpSyn` synapses). Each simulation had a time step dt=0.01ms and a length of 10s, the simulation was repeated over 4 seeds to yield a mean and a standard deviation in the estimate of the membrane potential fluctuations at the soma (see Figure 3B).

V.5 Analytical derivation of the fluctuation properties: strategy

We present here a derivation that provides an analytical approximation for the properties of the fluctuations of the membrane potential at the soma for our model. Summing up its properties, we get: 1) a morphology with a lumped somatic compartement and a dendritic tree of symmetric branching following Rall's rule 2) conductance-based synapses 3) independent excitatory and inhibitory shotnoise input spread all over the morphology 4) assymetric properties between a proximal part and a distal part and 5) a certain degree of synchrony in the pre-synaptic spikes.

The properties of the membrane potential fluctuations at the soma correspond to three stationary statistical properties of the fluctuations: their mean μ_V, their standard deviation σ_V and their *global* autocorrelation time τ_V. Following Zerlaut et al. (2016), we emphasize that the *global* autocorrelation time is a partial description of the autocorrelation function (as the autocorrelation function is not exponential) but it constitutes the first order description of the temporal dynamics of the fluctuations.

A commonly adopted strategy in the *fluctuation-driven* regime to obtain statistical properties is to use stochastic calculus after having performed the *diffusion approximation*, i.e. approximating the synaptic conductance time course by a stochastic process, see e.g. (Tuckwell et al., 2002)). This approach is nonetheless not easily generalizable to conductance input in an extended structure and render the inclusion of assymetric properties (proximal vs distal) complicated. We rather propose here an approach that combines simplifying assumptions and analytical results from shotnoise theory, it

constitutes an extension of the approach proposed in Kuhn et al. (2004).

For each set of synaptic stimulation $\{\nu_p^e, \nu_i^p, \nu_e^d, \nu_i^d, s\}$, the derivation corresponds to the following steps:

- We transform the dendritic structure to its equivalent cylinder. The reduction to the equivalent cylinder is "activity-dependent" and captures the changes in membrane properties that results from the mean synaptic conductance levels.

- We derive a mean membrane potential $\mu_V(x)$ corresponding to the stationary response to constant densities of conductances given by the means of the synaptic stimulation. We use this space-dependent membrane potential $\mu_V(x)$ to fix the driving force all along the membrane for all synapses. The relation between synaptic events and the membrane potential now becomes linear.

- We derive a new cable equation that describes the variations of the membrane potential around this $\mu_V(x)$ solution.

- We calculate the effect of one synaptic event on a branch $b, b \in [1, B]$ at a distance x. We calculate the post-synaptic membrane potential event $\mathrm{PSP}_b(x, t)$ at the soma resulting from b synchronous synaptic events occuring at the distance x from the soma. We approximate the effect of only one event by rescaling the response by the number of input $\mathrm{PSP}_b(x, t)/b$.

- We use shotnoise theory to compute the power spectrum density of the membrane potential fluctuations resulting from all excitatory and inhibitory synaptic events (including the synchrony between events).

The full derivation has been conducted with the help of the python modulus for symbolic computation: `sympy` (deriving homogenous solutions is relatively simple but computing coefficients with the bouaries conditions give rise to complex expressions because of the number of parameters). The resulting expression were then exported to `numpy` functions for numerical evaluation. The `ipython` notebook that presents the full derivation is available on the following link.

V.6 From fluctuation properties to spiking probability

Focus of a previous communication, see Zerlaut et al. (2016).

Reduced dataset n=27 cells, We remove the cells that had too low or too high excitabilities firing rates

Hard to conduct an anlysis on 7 orders of magnitudes from $\nu \in [10^{-5}, 10^2]$Hz, here restricting it to $[10^{-1}, 10^1]$Hz

V.7 Experimental preparation and electrophysiological recordings

Experiments were performed at Unité de Neurosciences, Information et Complexité, Gif sur Yvette, France. Experimental procedures with animals were performed following the instructions of the European Council Directive 2010 86/609/EEC and its French transposition (Décret 2013/118). Experimental methods were identical to those presented in Zerlaut et al. (2016). Very briefly, we performed intracellular recordings in the current-clamp mode using the perforated patch technique on layer V pyramidal neurons of coronal slices of juvenile mice primary visual cortex. For the n=13 cells presented in this study, the access resistance R_S was *XX* MΩ $\pm$ *YY*, the leak current at -75mV was *XX* pA $\pm$ *YY*, cells had an input

resistance R_m of *XX* MΩ ± *YY* and a membrane time constant at rest of *XX* ms ± *YY*.

V.8 Input impedance characterization

To determine the input impedance at the soma, we injected sinusoidal currents in the current-clamp mode of the amplifier (Multiclamp 700B, Molecular Devices), we recorded the membrane potential response to a current input of the form $I(t) = I \sin(2\pi f t)$, we varied the frequencies f and amplitudes $I over 40 episodes per cell. The frequency range scanned was [0.1, 500] Hz. For each cell, we determined manually the current amplitude I_0 that gave a ~ 5mV amplitude in a current step protocol, from this value, the value of I was scaled exponentially between I_0 at 0.1 Hz and $50I_0$ at 500Hz. The reason for varying the current amplitude (and not only the oscillation frequency) in those input impedance protocols is to anticipate for the low pass filtering of the membrane and insure that the membrane potential response at high frequencies is far above the electronic noise level (~ 0.1 mV).

After removing the first 3 periods of the oscillations (to avoid transient effects), we fitted the membrane potential response to the form:

$$V(t) = E_L + R\,I\,\sin(2\pi f t - \phi) \tag{11}$$

where E_L, R and ϕ were fitted with a least-square minimization procedure. The frequency dependent values of R and ϕ give the modulus and phase shift of the input impedance presented in Figure 2A.

write formula of the theoretical model for comparison !

V.9 Fitting passive properties and a mean morphology

Because the variables combined discrete (the branch number) and continuous variables, the minimization consisted in taking the minimum over a grid of paramters. The parameter space has 7 dimensions (given here with the considered range): the branch number ($B \in [2, 7]$), the somatic length ($L_S \in [5, 20]\mu$m), the total length of the tree ($L_t \in [300, 800]\mu$m), the diameter of the root branch ($D_t \in [0.5, 4]\mu$m), the leak specific resistance ($r_m \in [100, 1000]\mu S/cm^2$), the intracellular resistivity ($r_i \in [10, 90]\Omega.cm$), the specific capacitance ($c_m \in [0.8, 1.8]\mu F/cm^2$).

Each dimension was discretized in 5 points, the scan of the 7 dimensional space then consisted in finding the least square residual of the product of the modulus and phase of the impedance over this 5^7 points. The resulting parameters are shown on Table 1.

VI Supplementary information

VI.1 Supplementary material

Supplementary material contains the detailed mathematical derivation of the membrane potential fluctuations

VI.2 Acknowledgments

VI.3 Funding

VI.4 Author contributions

Y.Z. and A.D. designed research. Y.Z performed research and wrote the present draft.

VII References

Baudot P, Levy M, Marre O, Monier C, Pananceau M, Frégnac Y (2013) Animation of natural scene by virtual eye-movements evokes high precision and low noise in V1 neurons. *Frontiers in neural circuits* 7:206.

Crochet S, Poulet JFA, Kremer Y, Petersen CCH (2011) Synaptic mechanisms underlying sparse coding of active touch. *Neuron* 69:1160–1175.

Destexhe A, Mainen ZF, Sejnowski TJ (1998) Kinetic Models of Synaptic Transmission.

Destexhe A, Rudolph M, Paré D (2003) The high-conductance state of neocortical neurons in vivo. *Nature reviews. Neuroscience* 4:739–751.

El Boustani S, Destexhe A (2009) A master equation formalism for macroscopic modeling of asynchronous irregular activity states. *Neural computation* 21:46–100.

Hines ML, Carnevale N (1997) The NEURON simulation environment. *Neural computation* 9:1179–209.

Kuhn A, Aertsen A, Rotter S (2004) Neuronal integration of synaptic input in the fluctuation-driven regime. *The Journal of neuroscience : the official journal of the Society for Neuroscience* 24:2345–56.

Magee JC (2000) Dendritic integration of excitatory synaptic input. *Nature reviews. Neuroscience* 1:181–190.

Okun M, Steinmetz NA, Cossell L, Iacaruso MF, Ko H, Barthó P, Moore T, Hofer SB, Mrsic-Flogel TD, Carandini M et al. (2015) Diverse coupling of neurons to populations in sensory cortex. *Nature* 521:511–515.

Peyrache A, Dehghani N, Eskandar EN, Madsen JR, Anderson WS, Donoghue Ja, Hochberg LR, Halgren E, Cash SS, Destexhe A (2012) Spatiotemporal dynamics of neocortical excitation and inhibition during human sleep. *Proceedings of the National Academy of Sciences of the United States of America* 109:1731–6.

Rall W (1962) Electrophysiology of a dendritic neuron model. *Biophysical journal* 2:145.

Rauch A, La Camera G, Lüscher HR, Senn W, Fusi S, Luscher HR (2003) Neocortical Pyramidal Cells Respond as Integrate-and-Fire Neurons to In Vivo-Like Input Currents. *J Neurophysiol* 90:1598–1612.

Rossant C, Leijon S, Magnusson aK, Brette R (2011) Sensitivity of Noisy Neurons to Coincident Inputs. *Journal of Neuroscience* 31:17193–17206.

Spruston N (2008) Pyramidal neurons: dendritic structure and synaptic integration. *Nature reviews. Neuroscience* 9:206–21.

Tuckwell HC, Wan FYM, Rospars JP (2002) A spatial stochastic neuronal model with Ornstein–Uhlenbeck input current. *Biological cybernetics* 86:137–145.

Yang H, Kwon SE, Severson KS, O'Connor DH (2015) Origins of choice-related activity in mouse somatosensory cortex. *Nature neuroscience* 19:127–134.

Zerlaut Y, Telenczuk B, Deleuze C, Bal T, Ouanounou G, Destexhe A (2016) Heterogeneous firing response of mice layer V pyramidal neurons in the fluctuation-driven regime. *in revision* .